ISSN 1063-7761, Journal of Experimental and Theoretical Physics, 2018, Vol. 126, No. 1, pp. 83–89. © Pleiades Publishing, Inc., 2018.
Original Russian Text © R.M. Khusnutdinoff, B.N. Galimzyanov, A.V. Mokshin, 2018, published in Zhurnal Eksperimental'noi i Teoreticheskoi Fiziki, 2018, Vol. 153, No. 1, pp. 100–107.

SOLIDS
AND LIQUIDS

Dynamics of Liquid Lithium Atoms. Pseudopotential and EAM-Type Potentials

R. M. Khusnutdinoff*, B. N. Galimzyanov, and A. V. Mokshin**

Kazan (Volga region) Federal University, Kazan, 420008 Russia
**e-mail: khrm@mail.ru*
***e-mail: anatolii.mokshin@mail.ru*

Received August 22, 2017

Abstract—It is generally accepted that the complicated character of the interparticle interaction in liquid metals is reproduced most correctly by many-particle potentials of the EAM-type (embedded atom model) interparticle interaction. It is shown that in the case of liquid lithium near the melting temperature (T_m = 453.65 K), the spherical pseudopotential provides a better agreement with experimental data on elastic and inelastic X-ray scattering as compared to the known EAM potentials. The calculations of the dynamic structural factor and spectral densities of the longitudinal and transverse atomic currents lead to the conclusion that although the pseudopotential and EAM potentials generate a certain qualitative correspondence in the features of collective dynamics, the interparticle interaction of the spherical type reproduces correctly the general form of the dynamic structure factor in a certain wavenumber range, as well as the dispersion relation for collective excitations.

DOI: 10.1134/S1063776118010041

1. INTRODUCTION

Among other alkali metals, lithium has the simplest electronic structure $1s^2 2s^1$ (two inner s-electrons and one valence electron). According to the number of nucleon and electrons, lithium can be considered as the simplest metal existing in nature [1, 2]. Nevertheless, many properties of lithium melt are quite nontrivial, due to the specific ion–ion interaction [3], even as compared to other liquid alkali metals. For example, the potentials constructed on the basis of the local pseudopotential (e.g., Ashcroft potential [4]) for lithium cannot be used for reproducing the structure or dynamics, while such potentials for other alkali metals are in good agreement with experiments in a wide temperature range. This is partly due to the fact that the number of conduction electrons in lithium constitutes about 33% of their total number, while these fractions for sodium and cesium are 9% and 1.8%, respectively. Further, lithium practically does not mix with other alkali elements, while other alkali metals can form homogeneous mixtures (for example, we can mention sodium–potassium, cesium–rubidium, or cesium–potassium alloys) [5]. Lithium exhibits a higher chemical stability as compared to other alkali metals and forms compounds with many nonalkali metals, which are characterized by a high melting point and hardness [6]. Owing to its high specific heat and thermal conductivity, as well as low viscosity and density, liquid lithium can be effectively used as a coolant in uranium reactors in atomic power production [7].

For reproducing the interparticle interaction in liquid lithium, various model potentials were proposed, including local [8, 9] and nonlocal [10, 11] potentials, effective [12] spherical potentials (see review [13]), as well as many-particle EAM-type potentials (embedded atom method) [14, 15] and their modifications (modified embedded atom model, MEAM) [16]. Remarkably, in accordance with a large number of methods for developing interparticle interaction potentials, the potential parameters are selected from the very outset for reproducing correctly separate regions of the phase diagram as well as structural properties. Obviously, the "correct" structure does not imply the generation of the correct dynamics and transport properties by a potential. The main goal of this study is to analyze the accuracy of the description of the structure and the microscopic dynamics of liquid lithium in the vicinity of the melting temperature using different potentials of interparticle interaction, namely, the effective spherical pseudopotential [12], the embedded atom potential (many-particle EAM potential) [15], and modified embedded atom model potential (MEAM potential) [16].

2. STRUCTURE AND COLLECTIVE DYNAMICS OF LITHIUM ATOMS

We consider an equilibrium lithium melt at temperature T = 475 K with concentration $\rho = 0.0445$ Å^{-3}. Such a (ρ, T)-state is close to the melting curve, and its structure and collective atomic dynamics have investi-

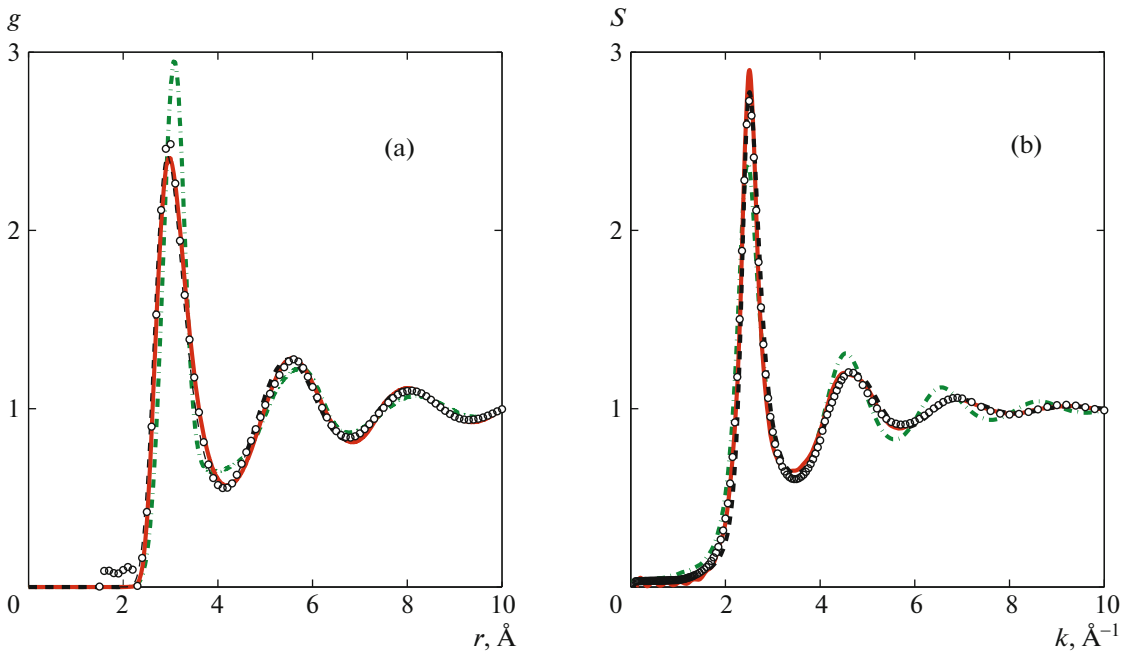

Fig. 1. (Color online) (a) Radial atomic distribution function for liquid lithium at temperature $T = 475$ K; the dashed, solid, and dot-and-dash curves are the results of simulation of the atomic dynamics with the effective pseudopotential [12], EAM potential [15], and modified embedded atom model (MEAM) potential [16], respectively; symbols are experimental data on X-ray diffraction [21]. (b) Static structure factor of the lithium melt.

gated experimentally quite extensively [17]. The system consists of $N = 4394$ particles in a cubic cell with periodic boundary conditions. As the initial conditions, we use the configuration of particles corresponding to the bcc lattice of crystalline lithium with lattice constant $a = 3.555$ Å and with zero velocities and accelerations. We consider three different model interparticle interaction potentials: spherical pseudopotential [12], many-particle EAM potential [15], and the MEAM potential [16]. The details and characteristics of the potentials used here are given in Appendix. The equations of motion are integrated using the Verlet algorithm in the velocity form with time step $\tau = 10^{-15}$ s [18]. To bring the system to thermodynamic equilibrium and to calculate the spectral characteristics, 100000 and 2000000 time steps have been made, respectively.

2.1. Structural Features of Lithium Melt

As mentioned in Introduction, the most widely used method to verify the accuracy of the interatomic interaction potential is the calculation of the radial atomic distribution function [19, 20]

$$g(r) = \frac{V}{4\pi r^2 N}\left\langle \sum_i \frac{\Delta n_i(r)}{\Delta r} \right\rangle \quad (1)$$

and the static structure factor

$$S(k) = 1 + \frac{N}{V}\int [g(r) - 1]\exp(i\mathbf{k}\cdot\mathbf{r})d\mathbf{r} \quad (2)$$

as well as the comparison of the values of these quantities with experimental X-ray diffraction data [21]. Here, V is the volume of the system; $\mathbf{k}$ and $\mathbf{r}$ are the wavevector and the radius vector that determines the position of the particle, and $\Delta n_i(r)$ is the number of particles in a spherical layer of thickness Δr at distance r from the ith particle.

In Fig. 1, functions $g(r)$ and $S(k)$ for liquid lithium at temperature $T = 475$ K, which are calculated using different interatomic interaction potentials, are compared with the experimental X-ray diffraction data [21]. It can be seen from the figures that the two model potentials (pair pseudopotential [12] and EAM potential [15]) are generally in better agreement with experimental data on X-ray diffraction [21] as compared to the MEAM potential [16].

2.2. Microscopic Collective Dynamics of Liquid Lithium

The collective dynamics of a many-particle system is characterized by the experimentally determined quantity, viz., dynamic structure factor $S(k, \omega)$. The quantity $S(k, \omega)$ can also be determined from the trajectories of particles, which are estimated from molecular dynamics simulations [22]:

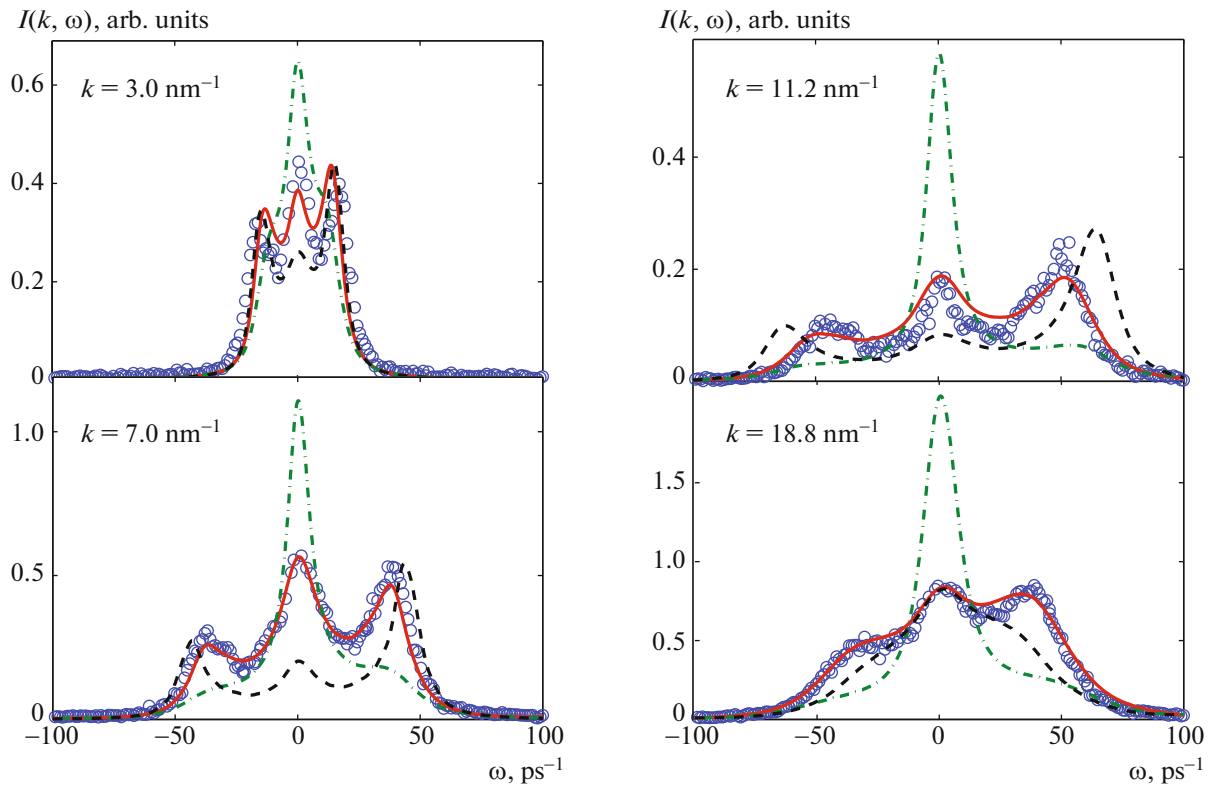

Fig. 2. (Color online) X-ray scattering intensity in lithium melt at temperature $T = 475$ K; symbols are experimental data on inelastic scattering of X-rays [23]. The solid, dashed, and dot-and-dash curves show the results of simulation of the atomic dynamics with the effective pseudopotential [12], EAM potential [15], and modified embedded atom model (MEAM) potential [16], respectively. For comparison of theoretical curves with experimental data, the results of simulation were transformed taking into account the experimental resolution function from formula (4) and Eq. (5).

$$S(k,\omega) = \frac{1}{2\pi N}\int_{-\infty}^{\infty} e^{-i\omega t}\sum_{l,j}\langle \exp[-i\mathbf{k}\cdot\mathbf{r}_l(0)]\exp[i\mathbf{k}\cdot\mathbf{r}_j(t)]\rangle dt. \quad (3)$$

Here, the angle brackets indicate averaging over the number of particles and time samplings.

To compare the results of simulation with experimental data, we computed the X-ray scattering intensity spectra $I(k, \omega)$ for different values of wavenumber k. It should be noted that scattering intensity $I(k, \omega)$ is related to dynamic structure factor $S(k, \omega)$ as follows:

$$I(k,\omega) = E(k)\int R(k,\omega-\omega')S_q(k,\omega')d\omega', \quad (4)$$

$$S_q(k,\omega) = \frac{\hbar\omega/k_\mathrm{B}T}{1-\exp(-\hbar\omega/k_\mathrm{B}T)}S(k,\omega), \quad (5)$$

where $S_q(k, \omega)$ is the quantum dynamic structure factor, $E(k)$ is the normalization factor, and $R(k, \omega)$ is the experimental resolution function, which is the intensity of scattering by an empty container.

In Fig. 2, the X-ray scattering spectra for liquid lithium in the vicinity of the melting temperature [23] are compared with the molecular dynamics simulation results obtained with different interatomic interaction potentials. It is quite unexpected that the simulation results with the spherical pseudopotential [12] are in complete agreement with experimental data on X-ray scattering and reproduce all features of the $I(k, \omega)$ spectra. At the same time, the results of simulation with the EAM potential [15] and MEAM potential [16] show considerable discrepancy with experimental data.

For detailed analysis of acoustic collective excitation of longitudinal and transverse polarizations in liquid lithium near the melting temperature, we calculated the spectral densities

$$\tilde{C}_\alpha(k,\omega) = \frac{k_\mathrm{B}T}{\pi m}\int_0^\infty C_\alpha(k,t)e^{-i\omega t}dt, \quad \alpha = L,T \quad (6)$$

(m is the particle mass) of normalized time correlation functions of the longitudinal current,

$$C_L(k,t) = \frac{\langle(\mathbf{e}_k\cdot\mathbf{j}^*(k,0))\mathbf{e}_k\cdot(\mathbf{e}_k\cdot\mathbf{j}(k,t))\mathbf{e}_k\rangle}{\langle|\mathbf{e}_k\cdot\mathbf{j}(k,0)|^2\rangle}, \quad (7)$$

as well as of the transverse current [24],

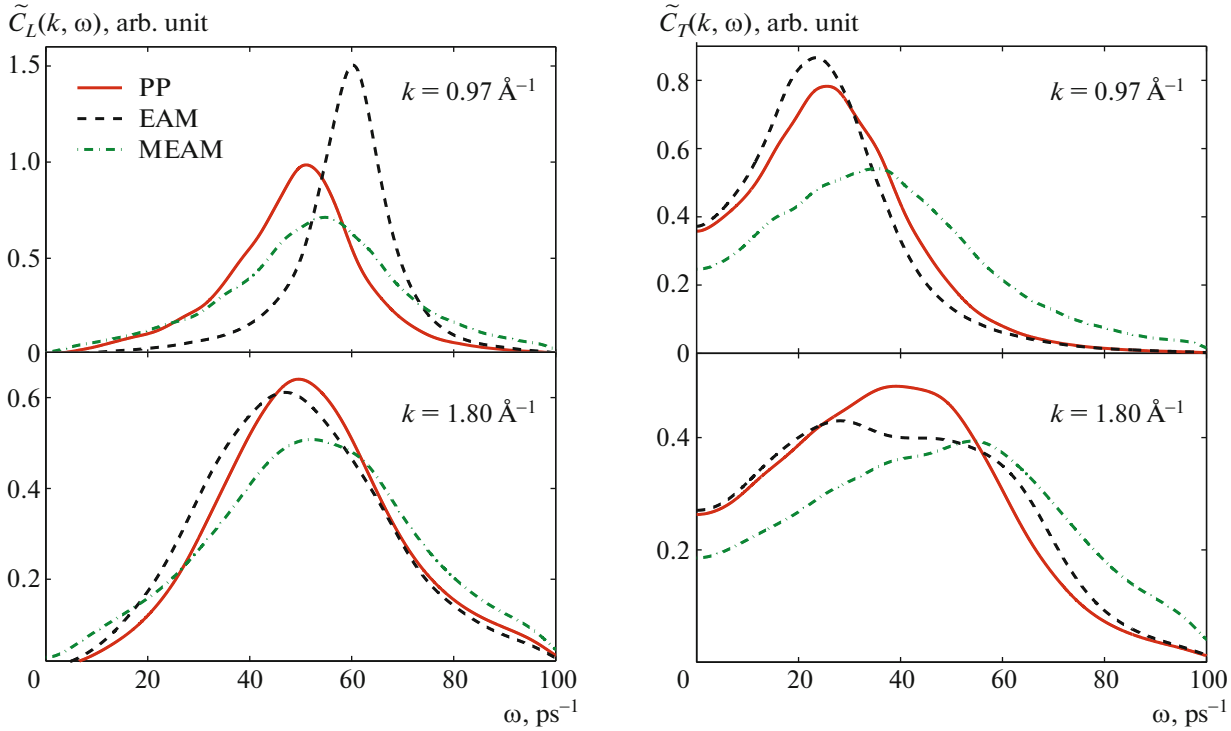

Fig. 3. (Color online) Spectral densities of time correlation functions $\tilde{C}_L(k, \omega)$ and $\tilde{C}_T(k, \omega)$ of the longitudinal and transverse currents, respectively, for the lithium melt at temperature $T = 475$ K, which were obtained from the results of simulation of the atomic/molecular dynamics with the pair effective pseudopotential (solid curves) [12], and many-particle EAM and MEAM potentials (dashed and dot-and-dash curves, respectively) [15, 16].

$$C_T(k,t) = \frac{\langle([\mathbf{e}_k \times \mathbf{j}^*(k,0)] \cdot [\mathbf{e}_k \times \mathbf{j}(k,t)])\rangle}{\langle|\mathbf{e}_k \times \mathbf{j}(k,0)|^2\rangle}. \quad (8)$$

Here, the parentheses and brackets indicate the scalar and vector products, respectively; quantity $\mathbf{j}(k, t)$ is the microscopic mass current, which is defined as [25]

$$\mathbf{j}(k,t) = \frac{1}{\sqrt{N}}\sum_{l}^{N} \boldsymbol{\vartheta}_l(t)\exp(-i\mathbf{k}\cdot\mathbf{r}_l(t)), \quad (9)$$

where $\boldsymbol{\vartheta}_l(t)$ is the velocity of the lth particle at instant t and $\mathbf{e}_k = \mathbf{k}/|\mathbf{k}|$. Figure 3 shows the frequency spectra $\tilde{C}_L(k, \omega)$ and $\tilde{C}_T(k, \omega)$ for the range of wavenumbers corresponding to $k < k_m/2$ and $k > k_m/2$. Here, $k_m/2 = 1.25$ Å is the boundary of the first Brillouin pseudozone and $k_m = 2.5$ Å^{-1} is the position of the principal peak of static structural factor $S(k)$. It can be seen from the figure that the peaks are manifested clearly in the spectra $\tilde{C}_L(k, \omega)$ and $\tilde{C}_T(k, \omega)$ in the high-frequency region for all three model potentials. At the same time, the lineshapes of the spectra, as well as the positions of the peaks and their heights (for a fixed k), exhibit clearly manifested differences for different potentials.

Figure 4 shows the dispersions of collective excitations of the longitudinal and transverse polarizations of liquid lithium, which were obtained from calculated spectra[1] $\tilde{C}_L(k, \omega)$ and $\tilde{C}_T(k, \omega)$ and experimental dependences $I(k, \omega)$. As can be seen from Fig. 4a, the simulation results for low values of the wavenumbers are in good agreement with the experimental data on X-ray scattering [23]. In addition, the results of calculations and the experimental data indicate the so-called positive dispersion effect for the velocity of sound in the microscopic region ($k < k_m/2$), when the values of $\omega_c^{(L)}(k)$ exceed the value predicted by the hydrodynamic theory [26, 27] with linear dispersion $\omega_c^{(L)}(k) = c_s k$, where $c_s = 4554$ m/s is the adiabatic velocity of sound. At the same time, Fig. 4a shows that the simulation results with the pair pseudopotential [12] are in better agreement with experimental data [23] as compared to the results of calculations obtained on the basis of many-particle potentials [15, 16].

Figure 4b shows the simulation results for the dispersion relation of collective excitations for transverse polarization $\omega_c^{(T)}(k)$. Since experimental data for $\omega_c^{(T)}(k)$ for liquid lithium near the melting temperature

[1] Note that the spectral density of the time correlation function of the longitudinal mass current is connected with the dynamic structure factor by the relation $\tilde{C}_L(k, \omega) = (\omega^2/k^2)S(k, \omega)$,

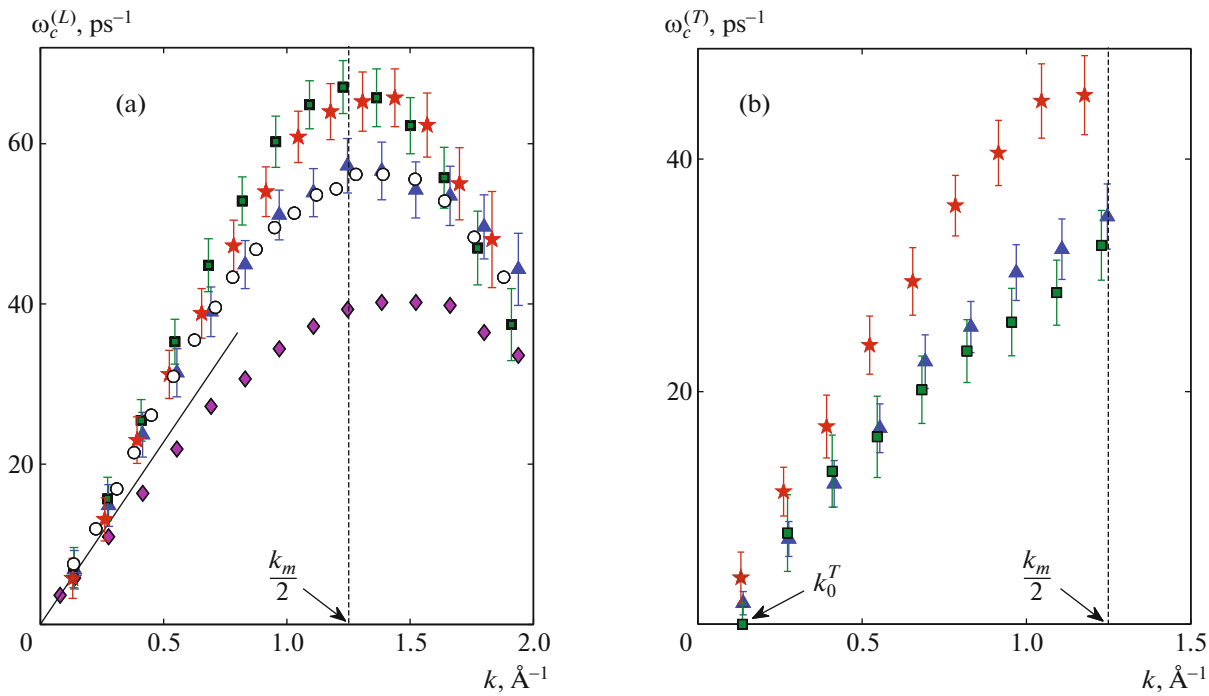

Fig. 4. (Color online) (a) Dispersion relation of collective excitations of the longitudinal polarization for lithium melt at temperature $T = 475$ K; ▲, ■, and ★ are the results of simulation with the effective spherical pseudopotential [12], EAM potential [15], and modified embedded atom model (MEAM) potential [16], respectively; ○ are experimental data on inelastic scattering of X-rays [23]; symbols ◆ correspond to frequency $\omega_0(k) = \sqrt{k_B T k^2/[mS(k)]}$ [21]. Dotted curve corresponds to $\omega_c^{(L)}(k) = c_s k$, where $c_s = 4554$ m/s is the adiabatic velocity of sound. (b) Dispersion relation for collective excitations of the transverse polarization for liquid lithium. Dashed lines mark the boundary of the first Brillouin pseudozone.

are not available, it is impossible to judge about the reliability of dispersion curves for the transverse polarization dynamics. Nevertheless, we can draw some qualitative conclusions. First, acoustic-like collective excitations of the transverse polarization with a characteristic dispersion relation are clearly manifested for all considered potentials in the collective dynamics of lithium atoms. Second, the extrapolation of the corresponding dispersion relation to the range of small values of k indicates the existence of the so-called gap of width k_0^T, in which $\omega_c^{(T)}$ assumes zero value [28].

3. CONCLUSIONS

We have performed molecular dynamics simulations of lithium melt at temperature $T = 475$ K ($T_m = 453.65$ K) with different model interparticle interaction potentials (spherical pseudopotential [12], EAM potential [15], and MEAM potential [16]). It is shown that the pair pseudopotential [12] and embedded atom (EAM) potential [15] correctly reproduce the "structural" features of the lithium melt near the melting point and correctly describe the experimental data on X-ray diffraction [21], while the simulation results based on the MEAM potential [16] exhibit substantial discrepancy with experimental data. It is found that the spherical pseudopotential reproduces the experimental data on X-ray scattering, as well as the dispersion of collective excitations of the longitudinal polarization in liquid lithium, most correctly in a wide range of wavenumbers. This result is rather unexpected since it means that a spherical-type potential can reproduce the ion–ion interaction of the lithium melt. The existence of propagating collective excitations of transverse polarization in the lithium melt near the melting point has been established.

APPENDIX

Interatomic Interaction Potentials

The *spherical effective pseudopotential* [12] is defined as the sum of the Coulomb interaction between ions and the electron-mediated contribution:

$$U(r) = \frac{Z^2}{r} + \phi(r), \tag{10}$$

where Z is the charge number. In turn, the Fourier transform $\phi(k) = FT[\phi(r)]$ is connected with pseudopotential $v(k)$ and the response function of the electron gas

Table 1. Some parameters of the EAM potential

n	$\bar{\rho}_n$	a_n, eV	b_n, eV	c_n, eV	g_n, eV Å^n	d_n
0	1.0	–	–	–	–1.615	–
1	0.9	–0.895	–	0.0326	32.92	0.253 eV
2	0.84	–0.894	–0.00652	1.7	–245.83	0.153 eV/Å
3	0.70	–0.888	–0.21052	–1.02	840.22	2.450 Å
4	0.55	–0.878	0.07508	1.75	–1369.38	0.380 eV
5	0.35	–0.850	–0.44992	–1.0	905.62	1.960 Å^{-1}
6	1.10	–0.800	–0.04992	11.0	–	–
7	–	–0.894	0.00652	0.0	–	–

$$\chi(k) = \frac{\chi^{(0)}(k)}{1 - \frac{4\pi}{k^2}[1 - G(k)]\chi^{(0)}(k)} \tag{11}$$

by the following relation:

$$\phi(k) = \chi(k)|v(k)|^2. \tag{12}$$

Here, function $G(k)$ takes into account the effects of exchange and correlation between electrons.

The *embedded atom potential* (many-particle EAM potential) [15] is defined by the expression

$$U = \sum_i \Phi(\bar{\rho}_i) + \sum_{i<j} \varphi(r_{ij}). \tag{13}$$

Here, $\varphi(r)$ is the pair interatomic interaction potential and $\Phi(\bar{\rho}_i)$ is the "embedding" potential of the ith atom, which depends on effective electron density $\bar{\rho}$. Electron density $\bar{\rho}_i$ for the ith atom is defined as [29]

$$\bar{\rho}_i = \sum_j \varrho(r_{ij}), \tag{14}$$

where

$$\begin{aligned} \varrho(r) &= p_1 \exp(-p_2 r), \\ p_1 &= 3.0511, \\ p_2 &= 1.22 \text{ Å}. \end{aligned} \tag{15}$$

Further, embedding potential $\Phi(\bar{\rho})$ is defined in terms of expressions corresponding to specific values of quantity $\bar{\rho}$:

$$\Phi(\bar{\rho}) = \begin{cases} a_1 + c_1(\bar{\rho} - \bar{\rho}_0)^2, \quad \bar{\rho}_1 < \bar{\rho} < \bar{\rho}_6, \\ a_i + b_i(\bar{\rho} - \bar{\rho}_{i-1}) + c_i(\bar{\rho} - \bar{\rho}_{i-1})^2, \\ \bar{\rho}_i < \bar{\rho} < \bar{\rho}_{i-1} \quad (i = 2,3,4,5), \\ a_6 + b_6(\bar{\rho} - \bar{\rho}_5) + c_6(\bar{\rho} - \bar{\rho}_5)^2, \quad \bar{\rho} < \bar{\rho}_5, \\ a_7 + b_7(\bar{\rho} - \bar{\rho}_6) + c_7(\bar{\rho} - \bar{\rho}_6)^{3/2}, \quad \bar{\rho} \geq \bar{\rho}_6. \end{cases} \tag{16}$$

The parameters required for this procedure are given in Table 1.

Finally, the pair interaction is defined as follows:

$$\varphi(r) = \begin{cases} d_1 + d_2(d_3 - r) + d_4(\exp[d_5(d_3 - r) - 1]), \\ r \leq 2.45 \text{ Å}, \\ g_0 + \frac{g_1}{r} + \frac{g_2}{r^2} + \frac{g_3}{r^3} + \frac{g_4}{r^4} + \frac{g_5}{r^5}, \\ r > 2.45 \text{ Å}. \end{cases} \tag{17}$$

The values of the parameters of this potential are given in Table 1.

In contrast to the EAM potential, the *modified embedded atom potential* (MEAM potential) [16] also contains the contribution taking into account three-particle interactions in the many-particle function (namely, in the embedding potential). This potential was proposed for describing 23 different elements, the ground state of which is characterized by different crystal lattices (fcc, bcc, and diamond cubic lattices). The MEAM potential is defined by the general expression

$$U = \sum_i \left[\Phi_i(\bar{\rho}_i) + \frac{1}{2} \sum_{j(\neq i)} \varphi_{ij}(r_{ij}) \right]. \tag{18}$$

Here, effective electron density $\bar{\rho}$ is given by

$$\bar{\rho} = \rho^{(0)} \sqrt{1 + \sum_{l=1}^{3} t^{(l)} \left(\frac{\rho^{(l)}}{\rho^{(0)}} \right)^2}, \tag{19}$$

where

$$\rho^{(l)} = \sqrt{\sum_i \sum_k \rho_l(r_{ik}) \sum_j \rho_l(r_{kj}) P_l^0(\cos(\theta_{ijk}))}, \tag{20}$$

$$\rho_l(r) = \exp[-\beta^{(l)}(r/r_0 - 1)], \tag{21}$$

$r_0 = 3/04$ Å is the distance between adjacent atoms, $P_l^0(\cos\theta)$ are associated Legendre polynomials, and $t^{(l)}$ and $\beta^{(l)}$ are the weight factors and damping coefficients for partial electron densities, which assume the following values: $t^{(1)} = 0.26$, $t^{(2)} = 0.44$, $t^{(3)} = -0.20$, and $\beta^{(0)} = 1.43$, $\beta^{(1)} = 1.0$, $\beta^{(2)} = 1.0$, $\beta^{(3)} = 1.0$.

The contribution connected with the embedding potential is defined in the form

$$\Phi(\bar{\rho}) = AE_c\bar{\rho}\ln\bar{\rho}, \quad (22)$$

where $A = 0.87$ is the scaling factor for the "embedding" energy and $E_c = 1.65$ eV is the sublimation energy.

Finally, the contribution associated with the pair potential is defined by the relation

$$\varphi(r) = \frac{2}{Z}[E^u(r) - \Phi(\bar{\rho}(r))], \quad (23)$$

where the energy of the atom of the corresponding standard structure,

$$E^u(r) = -E_c[1 + \alpha(r/r_0 - 1)]\exp[-\alpha(r/r_0 - 1)], \quad (24)$$

is taken into account, and $\alpha = 2.97$ is the damping constant for energy $E^u(r)$.

ACKNOWLEDGMENTS

Large-scale molecular-dynamic calculations were performed in the computer cluster of the Kazan Federal University and on the supercomputer of Interdepartmental Supercomputer Center of the Russian Academy of Sciences. The authors are grateful to Prof. L.E. Gonzälez (Universidad de Valladolid, Valladolid, Spain), who provided information (parameters and characteristics) on the liquid lithium pseudopotential. The authors are also grateful to the Ministry of Education and Science of the Russian Federation for supporting the research in the framework of the state assignment (no. 3.2166.2017/4.6). This work was also supported in part (molecular dynamics simulations) by the grant no. MD-5792.2016.2 from the President of the Russian Federation.

REFERENCES

1. N. H. March, *Liquid Metals: Concepts and Theory* (Cambridge Univ. Press, Cambridge, 1990).
2. A. V. Mokshin, R. M. Khusnutdinov, A. R. Akhmerova, and A. R. Musabirova, JETP Lett. **106** (6), 366 (2017).
3. W.-C. Pilgrim and Chr. Morkel, J. Phys.: Condens. Matter **18**, R585 (2006).
4. N. W. Ashcroft, Phys. Lett. **23**, 48 (1966).
5. *Handbook of Thermodynamic and Transport Properties of Alkali Metals* (Blackwell Scientific, Oxford, 1991).
6. N. M. Blagoveshchenskii, V. A. Morozov, A. G. Novikov, M. A. Pashnev, V. V. Savostin, A. L. Shimkevich, and O. V. Sobolev, J. Phys.: Condens. Matter **20**, 104201 (2008).
7. A. Fraile, S. Cuesta-López, R. Iglesias, A. Caro, and J. M. Perlado, J. Nucl. Mater. **440**, 98 (2013).
8. K. Hoshino and W. H. Young, J. Phys. F **16**, 1659 (1986).
9. T. Das and R. N. Joarder, J. Non-Cryst. Solids **117**, 583 (1990).
10. W. Jank and J. Hafner, J. Phys.: Codens. Matter **2**, 5065 (1990).
11. A. B. Walker and R. Taylor, J. Phys.: Condens. Matter **2**, 9481 (1990).
12. L. E. González, D. J. González, M. Silbert, and J. A. Alonso, J. Phys.: Condens. Matter **5**, 4283 (1993).
13. L. E. González, D. J. González, and J. M. López, J. Phys.: Condens. Matter **13**, 7801 (2001).
14. D. K. Belashchenko and O. I. Ostrovskii, High Temp. **47**, 211 (2009).
15. D. K. Belashchenko, Inorg. Mater. **48**, 79 (2012).
16. M. I. Baskes, Phys. Rev. B **46**, 2727 (1992).
17. T. Scopigno, G. Ruocco, and F. Sette, Rev. Mod. Phys. **77**, 881 (2005).
18. A. V. Mokshin, R. M. Yulmetev, R. M. Khusnutdinoff, and P. Hanggi, J. Exp. Theor. Phys. **103**, 841 (2006).
19. J. P. Hansen and I. R. McDonald, *Theory of Simple Liquids* (Academic Press, New York, 2006).
20. R. M. Khusnutdinoff, A. V. Mokshin, B. A. Klumov, R. E. Ryltsev, and N. M. Chtchelkatchev, J. Exp. Theor. Phys. **123**, 265 (2016).
21. Y. Waseda, *The Structure of Non-Crystalline Materials: Liquids and Amorphous Solids* (McGraw-Hill, New York, 1980).
22. A. V. Mokshin, R. M. Khusnutdinoff, A. G. Novikov, N. M. Blagoveshchenskii, and A. V. Puchkov, J. Exp. Theor. Phys. **121**, 828 (2015).
23. T. Scopigno, U. Balucani, G. Ruocco, and F. Sette, J. Phys.: Condens. Matter **12**, 8009 (2000).
24. W. Montfrooij and I. de Schepper, *Excitations in Simple Liquids, Liquid Metals and Superfluids* (Oxford Univ. Press, New York, 2010).
25. R. M. Khusnutdinoff and A. V. Mokshin, JETP Lett. **100**, 39 (2014).
26. J. P. Boon and S. Yip, *Molecular Hydrodynamics* (McGraw-Hill, New York, 1980).
27. R. M. Khusnutdinoff, A. V. Mokshin, S. G. Menshikova, A. L. Beltyukov, and V. I. Ladyanov, J. Exp. Theor. Phys. **122**, 859 (2016).
28. C. Yang, M. T. Dove, V. V. Brazhkin, and K. Trachenko, Phys. Rev. Lett. **118**, 215502 (2017).
29. A. V. Mokshin, A. V. Chvanova, and R. M. Khusnutdinoff, Theor. Math. Phys. **171**, 541 (2012).

Translated by N. Wadhwa